Rational design of reinforced rubber

D.J. Kohls, G. Beaucage*

Department of Materials Science and Engineering, University of Cincinnati, Cincinnati, OH 45221-0012, USA

Abstract

Filled elastomer systems have been studied extensively over the past several decades, especially in the application to tire performance. During this time, many attempts have been made to explain reinforcement of an elastomer when fillers are added. These reinforced properties include enhanced strength, modulus, abrasion resistance, and dynamic mechanical properties. Several approaches have been used to separate the contributing influences and to explain how they work. The majority of these approaches look at the structure and property relationships of the fillers and rubbers independently and as a synergistic combination. These approaches have evolved into the following major areas: filler structure, hydrodynamic reinforcement, and interactions involving fillers and elastomers. This paper will review the major works in each of these areas and attempt to offer an overall view of reinforcement of elastomers. Special attention will be paid to the relationships between filler structure and how it may be used to predict reinforcement properties. The general topics that will be covered included filler structure and characterization, rubber and filler interactions, mechanical reinforcement/hydrodynamic effect, and a fractal approach to explaining reinforcement.
© 2002 Elsevier Science Ltd. All rights reserved.

1. Introduction

Passenger car tires are composed of many different materials, e.g. steel belt, nylon fibers, gas barrier layers, to form an overall product. This paper will focus on re-inforcement of elastomers that are used in tire treads and side walls, emphasizing carbon and silica elastomer compounds. The elastomers are solution and emulsion styrene–butadiene rubber, natural rubber, and blends. Additives are used to increase the rubber's strength, wear resistance, performance and processing. These additives consist of fillers like carbon black and silica, curatives to promote cross-linking, mixing aids such as aromatic oil to aid the dispersion of fillers, and anti-degradants such as anti-oxidants and anti-ozonents. Already it can be seen that combining all of these materials together results in a complex composite with end properties depending on the formulation used. The processing of these materials also affects the end properties.

The resulting properties desired for filled rubbers include good mechanical properties, both static and dynamic, and tire specific properties such as traction, wear resistance, and rolling resistance. Typically these properties are obtained through a series of experiments that vary the ratios of additives and measure the effects. Recently however, efforts have been directed at understanding the mechanistic role of fillers in order to predict their effect on reinforcement.

2. Filler morphology and characterization

Studying the morphology and structure of fillers requires several techniques that probe a broad size scale (nm–μm) and describe different structural features. Fillers are made up of primary particles at the smallest size-scale, Angstrom to micron, which are strongly bonded to other primary particles to form an aggregated structure. The aggregates range from the nanometer to micron size-range and these can interact with other aggregates through weaker secondary bonding to form agglomerates. Tables 1 and 2 show the methods commonly used to determine filler morphology and how the morphologies relate to filler properties. These methods give information about the filler primary particle size, surface area, surface structure and energy aggregate size/structure, and agglomerate size/structure. This section will focus on 2 categories of filler characteristics: structure and surface area.

2.1. Structure

The structure of fillers is measured using electron

---

*Corresponding author. Tel.: +1-513-556-3096; fax: +1-513-556-2569.

E-mail address: jbeaucag@uceng.uc.edu (G. Beaucage).

Table 1
Filler characterization methods and information obtained

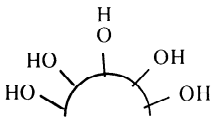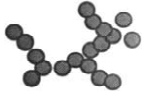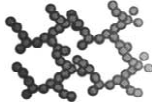| Method	Information
Scanning electron microscopy (SEM) Transmission electron microscopy (TEM)	Primary particle, aggregate and agglomerate structure, fractal geometry
Nitrogen gas absorption (N_2SA) Dibutyl phthalate absorption (DBPA) Cetyltrimethyl ammonium bromide absorption (CTAB)	Specific surface area, aggregate shape, particle size, pore size
X-Ray diffraction (XRD) Small angle X-ray scattering (SAXS) Small angle neutron scattering (SANS)	Primary particle, aggregate and agglomerate structure, surface area, fractal dimension
Infrared spectroscopy (IR) Nuclear magnetic resonance imaging (NMR) X-ray photo-spectroscopy (XPS) Inverse gas chromatography (IGC)	Filler surface structure and chemistry

microscopy, dibutyl phthalate (DBP) absorption, and small angle scattering (SAS). Each of these methods uses different sample preparation and looks at a different field of view or sample size which can give a difference in measured results for the same property, i.e. average vs. local properties.

Early work focused on characterizing carbon black by electron microscopy and DBP absorption. DBP absorption is based on measuring the amount of torque required to mix carbon black with *n*-dibutyl phthalate. By measuring the oil absorbed up to a pre-set torque level, information is given about the filler structure and is used to predict formulations for compounding. It gives an averaged result related to the structure of the carbon black. On the other hand, electron microscopy looks at only a few aggregates at a time. Medalia [1] used electron microscopy to predict the DBP absorption of carbon black and developed a model for the effective filler volume based on these results. The effective filler volume is considered to be the 'active' volume of the filler when added to an elastomer and is larger than the bulk volume fraction, ϕ, because of the branched structure of the aggregates. It is possible for

Table 2
Filler morphology and properties

	Morphology	Filler effect	Filler characterization
	Surface chemistry (Å size scale)	Filler–filler Filler–polymer	Surface functional groups
	Primary particle Volume, shape (Å–nm size scale)	Hydrodynamic/mechanical reinforcement	Size, shape Structure Surface area
	Branched aggregate (nm size scale)	Hydrodynamic Occluded rubber	Structure, Surface area Fractal dimension; branching coefficient
	Agglomerated Aggregates (nm–μm size scale)	Filler networking Trapped rubber	Structure Surface area Fractal dimension

rubber to be trapped in pores or voids of the aggregates which increases the effective filler volume, ϕ_{eff}. Medalia stated that this effective volume related to DBP absorption by:

$$\phi_{eff} = 0.5\phi[1 + (1 + 0.02139(DBP)/1.46] \qquad (1)$$

where ϕ is the actual volume fraction of filler. This relationship still holds as a predictor of the effective volume of carbon black.

In Medalia's work the individual aggregate morphology was studied with microscopy and correlated to the averaged structure properties measured by DBP. An equivalent sphere was calculated from the micrographs to describe the effective volume of the aggregate. The amount of rubber that could fill the voids within the equivalent sphere and between equivalent spheres was calculated. This information, along with the calculated size and packing of the spheres was used to predict DBP absorption and then to predict the effective filler volume. This is one of the first studies that used information on the filler structure to predict properties of the filled rubber. However, the equivalent sphere model was limited to filler volume fractions ($\phi < 0.15$), which is below the practical level for tire compounds. This is because it doesn't include the contribution of the agglomerates. Despite this limitation it was one of the first steps in explaining the reinforcing behavior of fillers based on structure.

Following Medalia's work, Gruber, Zerda, and Gerspacher [2] used TEM to describe the 3-dimensional structure of carbon black. They showed that the carbon black aggregates are planar, having a flat anisotropic dimension in one direction while also being highly branched. Fig. 1 is a schematic showing the anisotropic structure of carbon black. Electron microscopy is usually limited to characterizing structures in two dimensions. By collecting images of the carbon black aggregates at three different tilt angles Grüber attempted to describe the aggregates in three
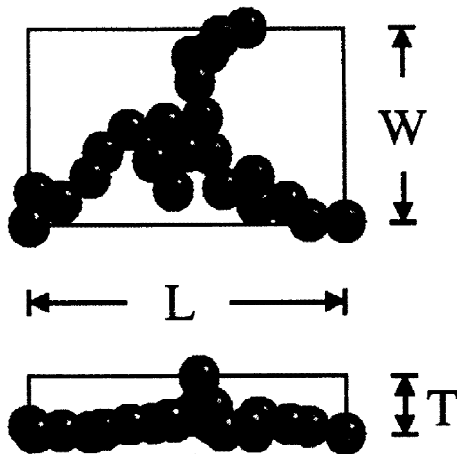
dimensions. Gruber explained that because of carbon black's branched structure (increased surface area) it is a good filler for reinforcement. However, he also mentions that by reducing the planarity of the carbon black the surface area could be increased and this could lead to even better reinforcing properties. To do this, it first must be understood why the carbon aggregates form such 3-dimensional structures, which has not been stated. This study shows that the morphology of carbon black is not isotropic. Because of this, the carbon black aggregates may have a preferred orientation in forming agglomerates or when dispersed in a rubber matrix. This study of carbon black dimension could be expanded to investigating the orientation of the aggregates in the rubber compound.

Many studies have been done using small angle X-ray scattering (SAXS) and small angle neutron scattering (SANS) to study the statistical 3-D structure of fillers like silica and carbon black [3–8]. Frölich and Göritz [3] reported using SAXS to study filled SBR rubber compounds using a fractal approach. They attempted to characterize the 3-dimensional structure and surface structure of carbon black aggregates. They did this through measurement of the mass fractal dimension d_m and the surface fractal dimension d_f of the aggregates in scattering experiments. The mass fractal dimension describes the scaling of mass with size of observation of an aggregated or porous material and the surface fractal dimension describes the smoothness or roughness of a 2-dimensional surface. Fig. 2 gives a description of both of these dimensions.

In Fig. 2 the compact mass fractal consists of a dense, completely filled structure while the fractal structure is branched and porous. For both, the mass, M, is a function of the radius of a sphere surrounding the structure and proportional to the radius raised to some power d_f. For the dense structure d_f is equal to 3. For the fractal structure d_f lies between 1 and 3 where 1 represents a linear (1-

Fig. 1. Dimensions of a carbon black aggregate.
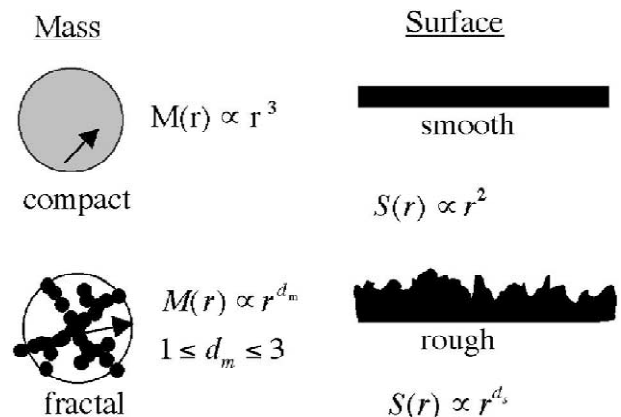
Fractal Structures

Fig. 2. Mass fractal and surface fractal structures [3].

dimensional) structure. While mass fractals describe 3-dimensional structures, surface fractals describe the 2-dimensional interface of a 3-dimensional structure. In Fig. 2, $S(r)$ is a function that evaluates the smoothness of the surface as a function of the length 'r'. If the specific surface area (S/mass) is constant across various lengths of observation, r, the surface is said to be smooth. If it changes as a function of r then the surface roughness is described by d_s which lies between 2 and 3. When $d_s = 2$, the surface is smooth; as d_s increases the surface increases in roughness [3].

To determine these dimensions, small angle scattering experiments were used by Frölich and Göritz combining SAXS and SANS results. In these experiments the samples are exposed to collimated radiation which is scattered at an angle 2θ and the number of counts (intensity) are recorded on a detector. The scattering angle 2θ is converted to a scattering vector, q, by:

$$q = \frac{4\pi \sin(\theta)}{\lambda} \tag{2}$$

A log–log plot of scattered intensity versus q is used to obtain a power law coefficient relating intensity to q by:

$$I_q \propto q^{-p} \tag{3}$$

For mass fractals, $p = d_m$ where q falls in the range of $2\pi/R < q < 2\pi/r_0$. R is the upper limit for the mass fractal structure and r_0 is the primary unit of the aggregate. For

surface fractals $p = 6 - d_s$ where q exceeds $2\pi/r_0$. The slope from a log–log plot gives the fractal dimension as shown in Fig. 3. This figure shows combined scattering curves from SANS, SAXS, and wide-angle X-ray diffraction (XRD). Since the regions where the slope changes for the mass fractal dimension occur at a lower q than the for the surface fractal dimension it is possible to distinguish these features from such a combined scattering plot.

Frölich and Göritz used this technique to study SBR rubbers filled with different grades of carbon black and silica. In their study they observed that the carbon blacks display apparently rough surfaces with surface fractal dimensions of 2.08–2.75. The carbon blacks also displayed a mass fractal dimension of 1.9–2.0. However, another study by Hjelm [6] interpreted the surface fractal regime as being due to polydispersity. Hjelm verified this interpretation with microscopy. It is unclear whether the surface of carbon black is smooth or rough. TEM images show a smooth carbon black surface while scanning tunneling microscopy (STM) shows a slightly rough surface. Fig. 4 shows the surface of carbon black N330 using STM and the carbon black aggregate structure using TEM. Beaucage et al. [8], have also noted the predictable influence of polydispersity on the apparent surface fractal scaling in conducting blacks.

The mass fractal dimension of carbon black has also been estimated by DBP absorption [10] and by TEM [11]. The surface fractal dimensions of a wide range of carbon blacks were also estimated by nitrogen absorption [12].
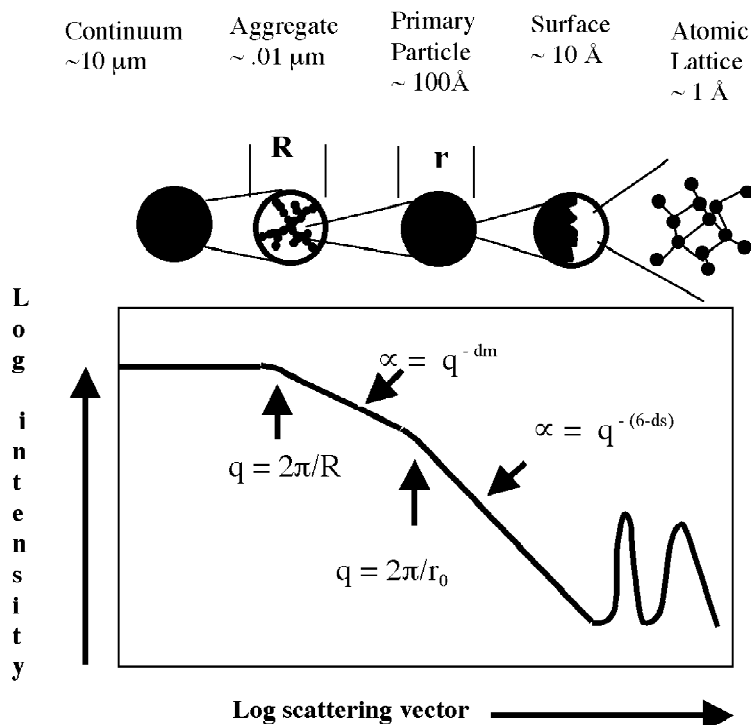

Fig. 3. Schematic of small angle scattering for aggregates, primary particles, and atomic structure [3].
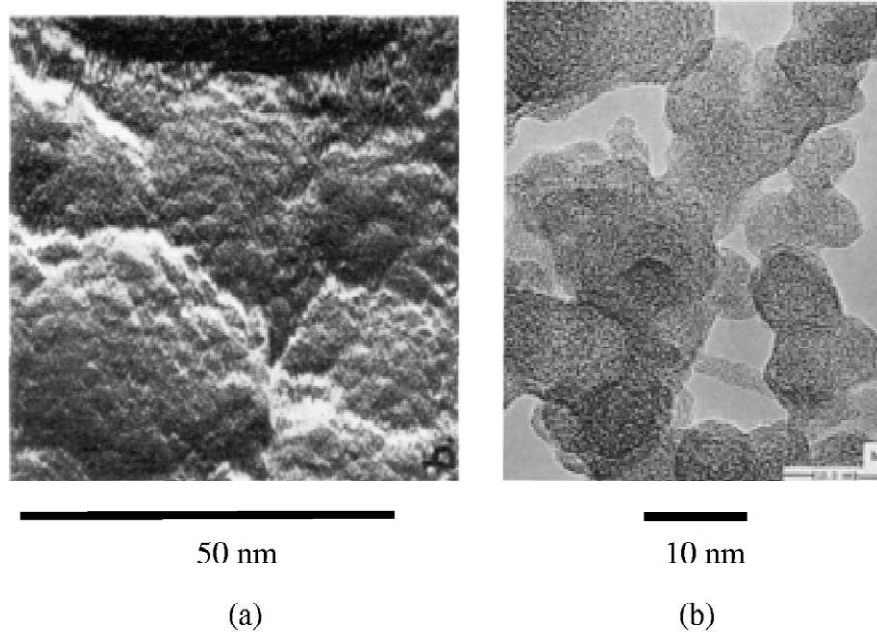
Fig. 4. (a) STEM of carbon black N330; (b) TEM of carbon black N220 [9].

Zerda [12] showed that the surface fractal dimension was independent of the type of carbon black with a value of 2.2±1, and Zerda's values differ from the studies by Hjem [6] and Frölich [3]. The difference in values can be explained by the experimental technique used. Scattering probes atoms on the surface and interior pores (closed pores) of the particles while nitrogen absorption measures only the surface of carbon black (open pores). These techniques should be looked at more closely and used together with models that predict reinforcement based on fractal dimensions. The literature is inconsistent and lacks sufficient comparison between techniques, especially in the use of microscopy to verify the existence of surface roughness for different grades of carbon black.

2.2. Specific surface area (SSA)

The specific surface area of fillers is studied because most fillers like carbon black and silica have branched porous structures. Because of their structure, they have a higher surface area than a compact dense spherical particle. This means that there is more of the filler available for interaction with the rubber. It has been clearly shown that fillers with different surface areas reinforce differently from one another. Table 1 shows the techniques used to measure specific surface area of fillers. The table includes nitrogen gas absorption (N_2SA) with Brunner Emmet Teller (BET) analysis and cetyltrimethyl ammonium bromide absorption (CTAB). The difference between nitrogen gas absorption or ammonium bromide absorption has to do with the size of the absorbent molecule. Nitrogen is a much smaller molecule that can penetrate smaller pores.

Because of this, nitrogen absorption tends to give a higher specific surface area value for highly structured fillers but roughly the same surface area for low structured fillers [13].

The specific surface area of a filler gives important information about the filler reinforcement properties, the total surface of particles and its pores. Fillers that are highly branched and that contain many pores tend to have higher specific surface areas and more locations to interact with the rubber matrix. Wang [14] has published a review on filler–elastomer interactions and he notes that the specific surface area of carbon black directly effects dynamic mechanical properties. Okel and Waddell [15] studied how the specific surface area of silica affects silica and carbon black filled rubbers. Both of these studies show that the specific surface area of the fillers affects mechanical properties and the processing of the compounds. When the surface area for silica increases there is a higher compound viscosity, which requires more energy (torque) for mixing and also contributes to the build up of heat in the mixture. If too much heat is generated the compound will cure prematurely. At the same time, as the filler surface area increases the tensile and tear strength of the rubber increases [15].

In general, measuring the specific surface area has been a standard practice in studying filled rubbers. Specific surface area information along with structure information about the filler can be combined to give some idea of how a rubber will be reinforced. Much is still unknown concerning the mechanisms of how these properties directly relate to reinforcement and what the exact mechanisms of reinforcement are.

3. Filler and rubber interactions

Interactions between fillers and rubbers have a significant effect on reinforcement properties of a filled rubber. The chemical and physical properties of both the rubber and filler as well as the amount of each present in a compound influence these interactions. Rubber–rubber interactions mainly occur when blends of rubber are used in compounds and are considered to be not as significant as filler–rubber and filler–filler interactions. Filler–rubber interactions are described by the compatibility of the filler with the rubber while filler–filler interactions are described by the attraction of a filler to itself and the ability to form a network. The most important effect of filler–rubber interactions has to do with the occlusion of rubber. So called 'bound rubber' is trapped between or within aggregates where it is no longer part of the elastically active rubber matrix. Instead, bound rubber acts as part of the filler network and increases the 'effective' filler volume.

Filler–filler interactions are a primary mechanism in reinforcement, especially at high filler loading. These interactions depend on chemical interactions between the filler particle surfaces (filler–filler, filler–rubber), physical interactions (van der Waals forces, hydrogen bonding), morphology of the filler network, and filler volume fraction. The surface energy of the filler influences how compatible it is with the rubber. Silica for example is highly polar and doesn't interact well with a non-polar elastomer like styrene–butadiene (SBR) but does have good interaction with polar elastomers like poly-dimethyl siloxane (PDMS). The filler structure also determines how compatible it is with the rubber. As the surface area of the filler increases it has more sites available to interact with the rubber or other filler particles. A highly branched structure also makes it possible for some of the rubber matrix to become mechanically interlocked between aggregates.

Filler–rubber interactions have been studied by Wolff and Wang in a series of papers on both carbon black and silica fillers [14,16–20]. Those studies looked at the effect of surface energy, distance between filler aggregates, and the effect of filler–rubber interactions on dynamic mechanical properties.

3.1. Surface energy

Wang and coworkers [14,16–18] have looked at filler–rubber interactions on the basis of surface energy for silica and carbon black. In one study [17] they compared a wide range of commercial carbon black and silica using inverse gas chromatography. This technique uses a stainless-steel column loaded with the filler particles. The technique is called 'inverse' gas chromatography because it is the column packing rather than the gas composition that is studied. Different organic vapors are passed through the column and their absorption by the filler is measured. The

basic equation used to describe the surface energy of fillers is:

$$\gamma_s = \gamma_s^d + \gamma_s^{sp} \qquad (4)$$

where γ_s = surface energy, γ_s^d = dispersive component, γ_s^{sp} = specific or polar component. Fillers with a high filler–filler interaction will have a high γ_s^{sp} and fillers with a high filler–rubber interaction will have a high γ_s^d. These energy terms have been measured for carbon black and silica by inverse gas chromatography using different hydrocarbon vapors. Carbon black has a high dispersive component with a stronger filler–rubber interaction and a weaker filler network. Silica has a high polar component and has a tendency to form a strong filler network and a weak filler–rubber network. One difference between carbon black and silica is in surface chemistry, shown schematically in Fig. 5. The surface of carbon black consists primarily of carboxyl (C=O) and carboxylic acid (C–OH) surface groups while silica has silanol (Si–OH) and silane (Si–OR) groups attached to the surface. The amount of silanol and silane can vary from pristine fumed silica ($\sim 100/m^2$) to precipitated silica ($\sim 100s–1000s/m^2$).

The study by Wang and coworkers [17] showed that the γ_s^d depends on the surface area of the carbon black but not on the structure. This was shown by comparing the surface area, as measured by nitrogen absorption, and a technique known as 24 M4 DBP absorption. 24 M4 DBP absorption is the same as DBP absorption except that the carbon black is crushed into a pellet and the absorption is measured. There was a direct relationship between the BET surface area and γ_s^d with γ_s^d; the surface energies increasing with increasing specific surface area. As the specific surface area of the aggregates increases there are more surfaces exposed compared to an aggregate of the same size but smaller surface area. However, the dependence of γ_s^d on structure could be investigated further with techniques besides 24 M4 DBP absorption. 24 M4 DBP absorption is problematic because it is possible to modify the pore structure of the carbon black through over packing of the aggregates. Investigations by small angle scattering would be interesting in confirming whether there is a relationship
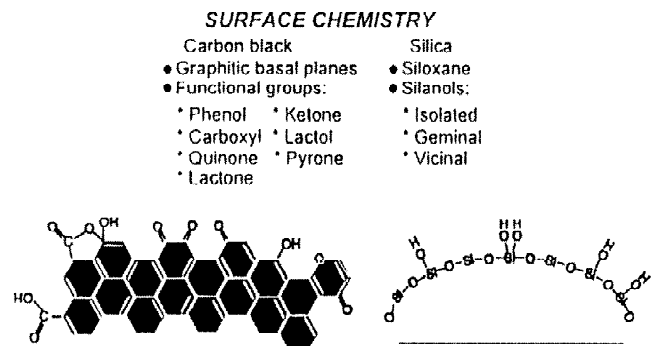

Fig. 5. Silica and carbon black surface chemistry [21].

between carbon black structure and surface area and γ_s^d. Similar relationships were shown for the specific component of surface energy γ_s^{sp}.

Wang [14] used surface energies to show how filler aggregates have a tendency to form either aggregates or agglomerates in the rubber matrix. He used a kinetic model for the change in adhesion energy based on Medalia's approach of chemical kinetics:

$$\Delta W = W_{ff} + W_{pp} - 2W_{fp} \tag{5}$$

where ΔW is the change in adhesion energy, W_{ff} is the adhesion energy between filler–filler, W_{pp} is the adhesion energy between polymer–polymer, and W_{fp} is the adhesion energy between filler and polymer. Each of these variables has a dispersive and specific component as described earlier in Eq. (4). According to Wang's model, when $\Delta W = 0$, the filler does not have a tendency to form agglomerates once the filler is dispersed in the rubber. When $\Delta W > 0$, the aggregates form agglomerates which are dispersed in the rubber matrix and when $\Delta W < 0$, the aggregates have a strong tendency to disperse in the rubber matrix without forming agglomerates.

Wang's model and similar models have been presented in studies on the effect of surface energy on filler–rubber interactions [18]. In one study, Wang and Wolff [18] relate the surface energies of fillers to elastomer reinforcement. They showed the dependency of bound rubber content, compound viscosity, and dynamic mechanical properties on the surface energies of the fillers. They chose a carbon black and silica filler with similar surface area and structure in order to compare the effect of different surface energies on reinforcement. It was shown that carbon black, which has a higher dispersive component, gave a higher bound rubber content and a higher modulus at high extension. This was due to the stronger filler–rubber interaction. Meanwhile, the silica had a higher viscosity during mixing, a higher dynamic modulus, and a higher modulus at low extensions. This indicated a strong filler network for silica because of the strong filler–filler interaction. While this study and the other studies, mentioned above, show that surface energy can be used to explain

reinforcement properties, there are other factors that may play significant roles as well. Studying the filler structure and surface area should compliment this study to help explain the formation of the filler network and the effect on reinforcement.

3.2. Bound rubber

Bound rubber is the rubber that is trapped by the filler aggregates after mixing. There are several models that explain the different ways in which rubber is excluded from the matrix and incorporated in with the filler. Fig. 6 illustrates these models. In case (a), the rubber chains are attracted either physically or chemically to form a rubber shell on the surface of the carbon black particle. The rubber that is attached closest to the carbon black molecule is much stiffer than the rubber molecules that are further away. In case (b), the rubber shell that is shown for the individual particle in (a) is seen throughout the filler aggregate. As in (a), the rubber chains closest to the aggregate are the stiffest. In this shell model bridging of the bound rubber in the aggregate leads to a higher bound rubber fraction. In case (c), rubber collects around the aggregate and the rubber shell to form an outer layer of occluded rubber. This layer is not as tightly bound to the filler aggregate but does experience decreased mobility near the surface of the aggregate. In case (d) rubber is trapped between aggregates which have formed an agglomerate. This rubber experiences little stiffness increase and becomes 'free' once the aggregate structure breaks apart during deformation.

These bound rubber models give an explanation of what happens when a filler network develops in the rubber but it is still not fully understood. Nuclear magnetic resonance imaging (NMR) studies have confirmed the existence of a rubber shell around filler particles [22]. This bound rubber affects the properties of the compounds by contributing to the filler volume to form an 'effective' filler volume fraction, ϕ_{eff}. Several factors affect the bound rubber content including: temperature; carbon black loading; CTAB surface area; and storage time of the rubber before it is cured.
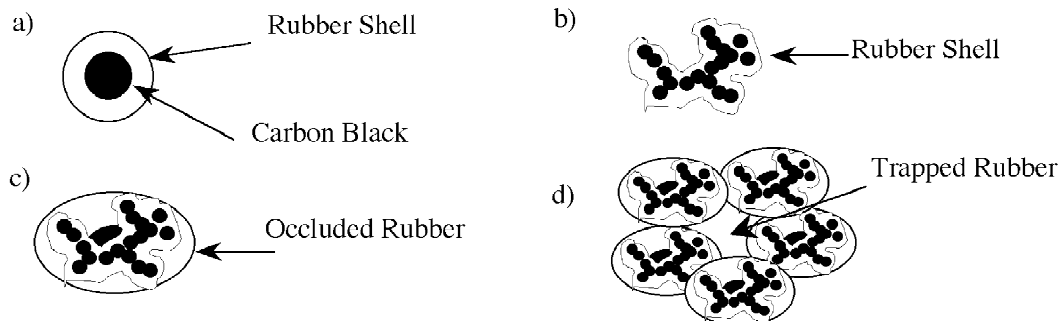

Fig. 6. Models of rubber excluded from the rubber matrix.

The bound rubber fraction of an uncured compound is the amount of rubber that is not extracted when it is exposed to a good solvent. Several studies have been published which show the factors that effect the bound rubber content for carbon black filled compounds. When the extraction takes place at a higher temperature the amount of bound rubber decreases which indicates that the bound rubber is physically rather than chemically bounded to the aggregates [23]. As the amount of carbon black is increased the bound rubber content also increases [24]. It was also shown that bound rubber content increases with increasing CTAB surface area of the carbon black [23]. Processing of rubber compounds also affects the bound rubber content. When the mixing time in increased during filler addition and when the storage time of the compound before curing is increased the bound rubber content also increases [21].

These studies show how sensitive the bound rubber content is to a variety of factors. The next section will discuss how the model of bound rubber is used to explain reinforcement mechanisms. It can be seen that the bound rubber content is determined by filler–rubber interactions through surface area, filler loading, and the physical absorption of the rubber to the aggregates. It should be noted that the bound rubber model has been determined empirically from many observations. However, the exact causes of bound rubber are not fully understood. The relationships between filler structure and the bound rubber content are also not known.

4. Reinforcement mechanisms

4.1. Hydrodynamic reinforcement

Several fundamental models can describe the mechanical reinforcement of rubber compounds. Among these, the simplest involves the hydrodynamic displacement of filler particles. This hydrodynamic effect has received attention and has been subject to modification in describing rubber reinforcement. Table 3 shows the evolving description of the hydrodynamic effect.

The hydrodynamic effect was first observed in the increased viscosity of a fluid with dispersed rigid particles. Einstein [25] explained this increase in viscosity with an equation relating the viscosity to the filler volume fraction ϕ, Eq. (6). One of the first steps taken to apply this effect in elastomers was to assume that the modulus of the rubber would behave similar to the viscosity of a liquid. This was done by Smallwood [26] with the assumption that the particles were spherical, dispersed, wetted, and under low shear stress. However, since the fillers do not meet these ideal conditions further modification was required, as shown in Table 3. Also for practical application the equation needed to be modified for higher filler fractions where filler–filler interactions are observed which introduced the ϕ^2 term. Guth and Gold [27] took into account the interactions of spherical fillers by adding an additional term in a power-series expansion, Eq. (7).

Eq. (7) has been modified in several ways to account for deviations of the fillers from the ideal case. In practice, fillers are not spherical but are asymmetric consisting of complex branched structures. Furthermore the hydrodynamic effect is limited to (1) small strains where the rigid filler provides the reinforcement; and (2) to low volume fractions to avoid filler–filler interactions. The next step took into account the deviation of the filler shape by a form factor 'f', introduced by Guth in Eq. (8). Medalia [28] described this equation by using an effective volume ϕ_{eff} in place of $f\phi$. The introduction of a structure factor 'f' and of the effective volume has been studied many times with variations of Eq. (8). The effect of occluded or bound rubber, filler shape, aggregate/agglomerate structure, and polymer–filler interactions have also been taken into account.

Wolff, Donnet, Wang, and coworkers have published many papers that discuss the hydrodynamic effect in rubbers [19,31,32]. The emphasis has been on obtaining appropriate expressions for the effective filler volume as it relates to occluded rubber. It is proposed that the aggregated geometry of filler leads to some of the rubber becoming 'trapped' within the filler voids. This trapped or occluded rubber acts to increase the effective volume of the filler. It was shown by Medalia [28] that this occluded rubber does not participate in the deformation of the reinforced rubber. Medalia related the modulus E of the rubber to the surface area (DBPA) of the filler previously shown in Eq. (1). Wolff and Donnet [31] replaced the modulus in Eq. (8) with the stress σ of the rubber under tensile stress–strain conditions. Using the data from the

Table 3
The historical development of the hydrodynamic effect

Equation	Modifications	Ref.
(6) $\eta = \eta_0(1 + 2.5\phi)$		[25,26]
(7) $E = E_0\left(1 + 2.5\phi + 14.1\phi^2\right)$	expanded ϕ^2 term	[27]
(8) $E = E_0\left(1 + 2.5f\phi + 14.1f^2\phi^2\right)$	f-structure factor, or $\phi_{\text{eff}} = f\phi$	[28]
(9) $G = G_0\left(1 + [G]\phi + \vartheta\phi^2\right)$	$[G] \propto R^{3-d_{\text{f}}}$	[29]
(10) $f = \dfrac{\eta}{\eta_0} = 1 + 2.5\phi + 10.05\phi^2 + A\exp(B\phi)$	A, B constants, $A = 0.00273$, $B = 16.6$	[30]

stress–strain experiments for rubbers filled with silica and carbon black they came up with values for the factor 'f' as a function of filler volume fraction (up to $\phi = 0.22$), temperature, and surface activity. While the data allowed for predicting the effective volume fraction by the factor: $\phi_{\text{eff}} = f\phi$, it was limited to extension modes and to volume fractions lower than 0.22.

The various models used to model the hydrodynamic effect have largely come about through numerous publications on experimental data that propose empirical relationships. Vilgis and Heinrich [33] have reviewed the area of reinforcement and emphasized that no consistent model exists that may be used to explain rubber reinforcement. Eggers and Schümmer [30] reported on the Thomas equation, Eq. (10), showing that it fit a much broader range of filler loading, $(0.1 < \phi < 0.5)$, than the previous forms of the Guth–Gold equation. However, as pointed out in the study by Eggers and Schümmer, these equations apply only to uncured systems. Once the rubber is vulcanized these models no longer apply.

So far, models have been proposed that explain the behavior of filled rubbers but are case specific and often look at a narrow range of fillers. The hydrodynamic effect accounts for the increase in modulus under conditions of low strain and low volume fraction. When the strain goes beyond a critical value, the majority of the modulus is attributed to the rubber itself. When the volume fraction of filler increases, filler–filler interaction increases and causes a filler network to form. This network causes reinforcement mechanisms different from those of simple hydrodynamics.

4.2. Dynamic mechanical reinforcement

Dynamic mechanical analysis is frequently used to measure the reinforcement of rubber by fillers. Dynamic mechanical testing is not a simple technique and the data from experiments are sensitive to the experimental set-up and testing conditions. This makes it difficult to directly compare results from one study to another. Also, individual experiments often give results that can only be compared relative to samples run under the exact same conditions and repeated several times. Despite these limitations, valuable data has been obtained from dynamic mechanical testing and trends can be seen that relate filler properties to mechanical reinforcement.

Wang reviewed several studies on filler reinforcement using dynamical mechanical analysis [14]. The major factors for dynamic reinforcement are filler structure, filler loading, and filler–rubber interactions. Each of these contribute to the occluded and trapped rubber in a compound. Dynamic mechanical testing can be carried out by varying the temperature, frequency, and strain imposed on a sample which has a direct impact on the filler–rubber network. Typically, two of these variables are held constant while the third is varied over a certain range. These experiments measure the dynamic stress–strain behavior of the materials and are expressed by a storage modulus G' and a loss modulus G''. Both of these are described by the stress and strain measured during the experiment where the stress is stated as:

$$\sigma = \sigma^o \sin \omega t \tag{6}$$

with ω being the frequency, t is time, and σ^o is the maximum stress. The strain is stated as:

$$\varepsilon = \varepsilon^o \cos(\omega t + \delta) \tag{7}$$

where ω is the frequency, t is time, ε^o is the maximum strain, and δ is the phase angle which is related to the difference in phase between the applied stress and the resulting strain.

The storage modulus, G', represents the elasticity of the rubber compound and is proportional to the work recovered after deformation and is described by:

$$G' = \left(\frac{\sigma^o}{\varepsilon^o}\right) \cos \delta \tag{8}$$

The loss modulus, G'', represents the viscous property of the compound and is proportional to the amount of work that is converted to heat during deformation and is described by:

$$G'' = \left(\frac{\sigma^o}{\varepsilon^o}\right) \sin \delta \tag{9}$$

Another parameter, tangent delta ($\tan \delta$) is the energy lost to the energy stored during cyclic deformation, which indicates the amount of hysteresis present during deformation and is described by:

$$\tan \delta = \frac{G''}{G'} \tag{10}$$

Plots of these three parameters as a function of temperature and dynamic strain amplitude (DSA) will give information about the filler network structure and filler–rubber interactions. Fig. 7 shows a plot of the storage modulus with temperature for rubbers with high, medium, and no filler loading. Wang [14] has explained the transition of the modulus with temperature in terms of the bound rubber. At low temperature the rubber matrix is glassy and little deformation occurs. As the temperature is increased the rubber matrix softens and goes through a glass transition temperature. At the low–medium temperature Wang proposes that the rubber shell around the aggregates begins to decrease. It is largest at the lowest temperature and extremely rigid but with increasing temperature it softens until a minimum layer remains. At high temperature the rubber shell has the same strength as the matrix and contributes little to reinforcement.

As the modulus begins to decrease with temperature, the rubber with the highest filler loading decreases the least while the gum rubber with no filler decreases the most. This feature was first described by Payne [34,35] and is
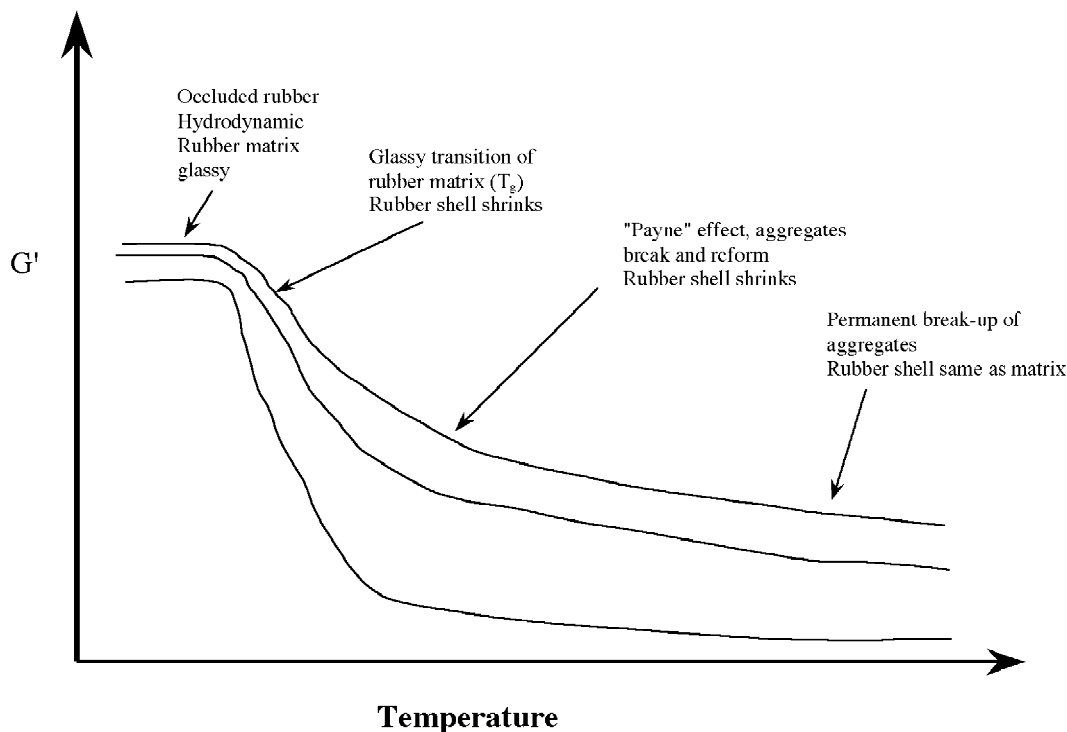
Fig. 7. The temperature dependence of G' for filled and unfilled rubbers.

known as the Payne effect. This effect is described and the break down and reformation of the filler network structure during dynamic mechanical testing. At moderate to high strain amplitudes the reformation of the network leads to an increased storage modulus. At sufficiently high strain amplitude the network is permanently broken and can no longer reform.

Wang used the Payne effect to also explain the what happens to the trapped rubber between aggregates. As the filler network breaks down and reforms, it is proposed that the trapped rubber is allowed to rejoin the rubber matrix and decrease the effective filler volume. The decreased effective filler volume causes the modulus to drop off even further at higher temperature or higher strain amplitudes. While this model of change in occluded rubber with temperature and strain amplitude seems to explain the changes occurring in filled rubber under dynamic testing, it is still an oversimplification for the effect of filler loading on reinforcement. Wang also looked at how filler surface area and structure influence dynamic mechanical behavior. It was found that increased surface area and higher filler structure increased the storage modulus. A rational explanation for these reinforcement mechanisms based on filler structure and filler loading is still lacking. It is currently the focus of several studies based on a fractal approach that attempts to predict the reinforcing properties of fillers [36,37].

5. Fractal explanation for reinforcement

Witten [29] describes the theoretical fractal geometry of fillers and relates it to reinforcing properties. Heinrich [36,37] and coworkers also describe the fractal relationship and compare it to experimental results. The occluded rubber that accounts for the effective volume fraction is described using several variables in Eq. (9) of Table 3: G_0 is the modulus of the rubber and $\vartheta\phi^2$ is a term of the order of ϕ^2. $[G]$ is the intrinsic modulus which is given by: $[G] \propto R^{3-d_f}$ where R is the aggregate size and d_f is the mass fractal dimension of the aggregate. This equation holds when the aggregates are significantly more rigid than the rubber.

Witten [29] has developed a model to explain the reinforcement mechanism. Heinrich [36,37] and coworkers used similar models and published data to confirm their predictions. These approaches will be summarized below.

At higher filler concentrations the filler can interpenetrate and overlap with sufficient mixing. Witten described this using the Ball–Brown modulus G_{BB} as shown in Eq. (11)

$$G_{BB} = E\phi^{(3+C)/(3-d_f)} \tag{11}$$

where C is the connectivity exponent, E is the tensile modulus of the filler material, and d_f is the fractal

dimension. The connectivity exponent, C, is related to the branching structure of fractal aggregates. The use of C and d_f was confirmed in the study by Heinrich and coworkers [36,37].

Under conditions of high strain and sufficient filler volume fraction, the higher strain of the filled rubber is achieved by stored elastic energy in the filler network. Witten proposed a scaling exponent for filled systems under high extension and strong uniaxial compression. The power law relationship Witten proposed relates the stress σ and strain λ by:

$$\sigma = E^* \lambda^P \tag{12}$$

where E^* is a constant. P depends on the strength of associations between aggregates and depends on d_f and C. Table 4 shows these relationships for various mechanical experiments.

Heinrich and coworkers have looked at filled systems from a fractal approach and used a percolation model to predict C and d_f. They looked at the dispersion and primary aggregate break up when the filler was above and below the network gel point ϕ^{**} and above and below percolation for conductivity ϕ^*. They also look at cluster growth below the gel point and at a kinetic cluster–cluster aggregation above the gel point. Similar to other theories they consider the polymer–polymer interactions as well as filler–filler interactions within each of these regions. They describe the formation of the filler network by looking at the fillers near the percolation threshold where the interactions can limit the network formation.

Similar to the approach of Witten [29], Henrich [36,37] applied fractal scaling laws to describe the filler network. They extend Witten's approach by defining three types of carbon black aggregates and their role in reinforcement. The primary structure $\phi_{A,1}$ consists of the smallest dispersable unit in the rubber. The secondary structure, $\phi_{A,2}$ consists of the growth of primary aggregates by cluster agglomeration. These agglomerates are weakly bonded. The third structure $\phi_{A,3}$ consists of the close packing of aggregates in a compact state. This structure is commonly seen when carbon black is compacted into pellets for processing of rubbers. Each of these structures are defined by a separate fractal dimension that ranges from about 3 for the compact aggregates to 1.8 for the cluster aggregates.

In order to describe the effects of these three filler structures, Heinrich [36,37] defines a dispersion rating D, which describes how well dispersed the filler is in the rubber matrix. This dispersion rating is related to an aggregation limit ϕ^+, volume fractions above which tenuous secondary aggregates form. This is an area to be explored further, to see how the structure of the aggregates affect the aggregation limit, ϕ^+, and how it contributes to the strength of the network.

Overall the use of fractals to explore the geometry of fillers is promising and through more experimentation these models can be tested. The fractal model offers an approach to organizing information about the filler and to relate it directly to mechanical properties.

6. Summary

This review has attempted to present a coherent picture of the often confusing and eclectic field of elastomer reinforcement especially as applied to tire tread compounds. Much progress has been made in recent years especially in terms of understanding structure–property relationships, dynamic mechanical testing, and fractal interpretation. This field appears to be at a standpoint for dramatic improvements in rational design with the goal of tunable properties aimed at improved tire performance.

References

[1] Medalia A. J Colloid Interface Sci 1970;32:115.
[2] Gruber T, Zerda T, Gerspacher M. Rubber Chem Technol 1994;67:280.
[3] Frölich J, Göritz D. Kautstuck Gummi Kunststoffe 1998;51:370.
[4] Reich M, Russo S, Snook I, Wagenfeld H. J Colloid Interface Sci 1990;135(2):353.
[5] Hurd A, Schaefer D, Smith D, Ross S, Le Mehaute A, Spooner S. Phys Rev Lett 1989;39:9742.
[6] Hjelm R, Wampler W, Seeger P, Gerspacher M. J Mater Res 1994;9:3210.

Table 4
Power relationship under tensile extension and uniaxial compression

High tensile extension		Strong uniaxial compression	
Weak associations	Strong associations	$d_f < 2C$	$d_f > 2C$
$P = 2(d_f - 1)/(C - d_f + 2)$	$P = (C + 1)/(C - 1)$	$P = -(C + d_f + 1)$	$P = -(3C + 1)/(2C - d_f + 1)$

D.J. Kohls, G. Beaucage / Current Opinion in Solid State and Materials Science 6 (2002) 183–194

[7] Gerspacher M, O'Farrell C. Elastomerics 1991;123(4):35.
[8] Beaucage G, Rane S, Schaefer DW, Long G, Fischer D. J Poly Sci, Part B: Polym Phys 1999;37:1105.
[9] Donnet J, Bansal R, Wang M. In: Carbon black, New York: Decker Inc, 1993, pp. 101–225.
[10] Herd C, McDonald G, Hess W. Rubber Chem Technol 1992;65:1.
[11] Ehrburger-Dolle F, Tence M. Carbon 1990;26:448.
[12] Zerda T, Yang H, Gerspacher M. Rubber Chem Technol 1993;66:130.
[13] Donnet J, Bansal R, Wang M. In: Carbon black, New York: Decker Inc, 1993, pp. 116–9.
[14] Wang M. Rubber Chem Tech 1998;71:521.
[15] Okel T, Waddell W. Rubber Chem Technol 1994;67:217.
[16] Wang M, Wolff S, Donnet J. Rubber Chem Technol 1991;64:558.
[17] Wang M, Wolff S. Rubber Chem Technol 1991;64:714.
[18] Wolff S, Wang M. Rubber Chem Technol 1992;65:329.
[19] Wang M, Wolff S, Tan E. Rubber Chem Technol 1993;66:178.
[20] Wolff S, Wang M, Tan E. Kautstuck Gummi Kunstoffe 1994;47:102.
[21] Leblanc J. J Appl Polymer Sci 1997;66:2257.
[22] Tstutsumi K, Ban K, Shibata K, Okazaki S, Kogoma M. J Adhesion 1996;57:45.
[23] Wolff S, Wang M, Tan E. Rubber Chem Technol 1993;66:163–77.
[24] Datta N, Choudhury N, Haidar B, Vidal A, Donnet J, Delmmotte L, Chezeau J. Polymer 1994;35(20):4293–339.
[25] Einstein A. Anna Phys Leipzig 1905;17:549.
[26] Smallwood HM. J Appl Phys Rev 1944;53.
[27] Guth E, Gold O. J Appl Phys 1945;16.
[28] Medalia A. J Colloid Interface Sci 1967;24:393.
[29] Witten T, Rubenstein M, Colby R. J Phys II France 1993;3:367.
[30] Egger H, Schümmer P. Rubber Chem Technol 1996;69:253.
[31] Wolff S, Donnet J. Rubber Chem Tech 1990;63:32.
[32] Wolff S. Rubber Chem Tech 1996;69:325.
[33] Vilgis T, Heinrich G. Macromolecules 1994;27:7846.
[34] Payne A. Rubber J 1964;146(1):36.
[35] Payne A. Rubber Chem Technol 1966;39:365.
[36] Klüppel M, Heinrich G. Rubber Chem Tech 1995;68:623.
[37] Klüppel M, Schuster R, Heinrich G. Rubber Chem Tech 1997;70:243.